Silicon
https://doi.org/10.1007/s12633-024-02992-z

RESEARCH

Synthesis of Analcime Zeolite from Glass Powder Waste and Aluminium Anodizing Waste

Luciano Fernandes de Magalhães[1] · Gilberto Rodrigues da Silva[1] · Andréia Bicalho Henriques[1] · Victor Augusto Araújo de Freitas[3] · Antônio Eduardo Clark Peres[2]

Received: 28 February 2024 / Accepted: 10 April 2024

Abstract
In this study, the 2-step hydrothermal synthesis of pure phase analcime zeolite from the combination of glass powder waste and aluminium anodizing waste was carried out, to contribute to the reduction of disposal of these industrial residues in sanitary landfills. Population growth has intensified industrial activities worldwide, increasing the generation of waste with a high potential for environmental impact. Currently, the reuse of solid wastes has become an alternative for the development of materials with greater added value. Placket Burman statistical design was used to identify the variables of greater statistical relevance in the synthesis process, aiming at future optimization. Crystallization time and temperature were verified as the most relevant variables in the synthesis, while calcination time and calcination temperature in the alkaline fusion step were the variables with less relevance. The results revealed the formation of single-phase analcime, reaching a crystallinity of up to 75% and a specific surface area of 43.3 $m^2.g^{-1}$. Scanning electron microscopy analysis showed the presence of particles with trapezoidal morphology, typical of analcime zeolite. Zeta potential measurement revealed an isoelectric point in pH 2.6, an important parameter in case of application in wastewater treatment. The investigated experimental conditions also enabled the formation of other zeolites, *e.g.*, Na-P1, cancrinite, and sodalite, demonstrating that the combination of glass powder waste and aluminium anodizing waste can be used to obtain different zeolitic phases. Consequently, products with greater added value can be obtained, contributing to sustainability in the aluminium and glass industries.

Keywords Analcime · Zeolite · Industrial residues · Circular economy · Hydrothermal synthesis

1 Introduction

Discovered in 1758 by the Swedish mineralogist Alex Fredrick Cronsted, zeolites are materials with microporous crystalline structures, which nowadays find application in several industrial sectors. These minerals, belonging to the class of aluminosilicates, are formed from the union of TO_4-type tetrahedrons, where T can be represented by the elements silicon and/or aluminium [1, 2]. The difference in valence between these two elements generates a crystal structure with an excess of negative electrical charge.

During its formation, the electrical charge is counterbalanced by compensation cations, usually elements of the alkali or alkali earth metal family [3]. Another peculiarity of these minerals is their microporous structure, which presents pores smaller than 20 Å, consequently resulting in a solid with a high surface area. The combination of these properties makes zeolites an attractive option for application as adsorbents [4–7], water softener [8, 9], catalysts in the petrochemical industry [10, 11], gas separation [12–14], medicine [15, 16], civil construction, as an addition to Portland cement [17–19], and many others.

Currently, more than 60 natural zeolite varieties are known, although large mineral deposits are relatively scarce [20]. With the increasing demand, studies indicated the feasibility of artificially replicating the conditions of zeolite formation in nature, and, from 1950 onwards, the mineral began to be synthesized on a large scale [21]. To date, more

✉ Luciano Fernandes de Magalhães
lucianofmag@demin.ufmg.br

[1] Department of Mining Engineering, Federal University of Minas Gerais, Belo Horizonte, MG, Brazil

[2] Department of Metallurgical and Materials Engineering, Federal University of Minas Gerais, Belo Horizonte, MG, Brazil

[3] Department of Natural Science, Federal University of São João del-Rei, São João del-Rei, MG, Brazil

Published online: 17 April 2024

than 230 different types of zeolites are currently known, being classified into 133 distinct crystal structures by the International Zeolite Association [22].

Among them, analcime is a naturally occurring zeolite that can also be synthesized. This zeolitic phase presents the chemical formula $Na_{16}Al_{16}Si_{32}O_{96}.16H_2O$ (framework type ANA) and is classified as a low-silica zeolite since the Si/Al ratio is less than 4 [23]. Low-silica zeolites present a high amount of aluminium in their chemical composition, increasing the negative electrical charge. Due to this, low-silica zeolites are materials with excellent adsorption and ion exchange capacities [24]. The crystalline structure of analcime is compact compared to other zeolites, exhibiting distorted pore sizes of 1.6×4.6 Å [25]. The analcime unit cell is composed of 24 cavities, and among them, 16 are filled with water molecules [26], which, theoretically, represent 8% of analcime weight. Table 1 summarizes the main physicochemical properties of analcime zeolite. Even possessing a small pore size, analcime still finds application in heavy metals adsorption, *e.g.,* lead, nickel, zinc, and copper [27], gas separation as a molecular sieve [28], and nuclear waste immobilization [28]. In any case, synthetic analcime displays higher efficiency compared to naturally occurring analcime due to the absence of other minerals and chemical elements that can act as contaminants [29].

Despite the possibility of producing synthetic zeolites, the process is costly, especially due to the chemical reagents used as a source of silicon and aluminium. An alternative approach is to use raw materials with high silicon and aluminium content as precursors, adding economic benefits to the synthesis, which encouraged the search for low-cost precursor materials [25, 31, 32]. In theory, any material rich in silicon and aluminium can be used as a precursor in the synthesis, even those considered residues from other industrial activities. Among the various industrial residues that can be used as sources of silicon and aluminium in the synthesis of analcime, glass powder waste (GPW) and aluminium anodizing waste (AAW) stand out for their chemical composition.

The glass powder is a silicon-rich waste generated during the cutting and polishing step in the production of glass pieces. Due to its fine particle size, this material is difficult to recycle, as it generates bubbles and imperfections in the new pieces [33]. It is estimated that the production of GPW accounts for approximately 5% of the total solid waste generated globally [34]. The disposal of GPW in landfills has become a common activity, and due to the low biodegradability of glass, this practice is considered harmful to the environment [35–38].

The electrochemical process responsible for the formation of an oxide layer on the surface of aluminium pieces, aiming at protection against corrosion is known as aluminium anodizing. The process takes place by immersing the aluminium pieces in a bath of NaOH and H_2SO_4, which removes part of the aluminium from the surface into the solution, generating a precipitate, the aluminium anodizing waste, that is separated and discarded. It is estimated that for every 1 ton of aluminium treated by anodizing, 475 kg of anodizing waste is generated, consisting mostly of aluminium oxyhydroxide [39, 40]. After solid–liquid separation, this residue, considered non-toxic and non-inert, is disposed of in landfills, and because of the alkalinity of this waste, significantly contributes to environmental impact [41].

When synthesizing zeolites from just one residue, the Si/Al ratio must be adjusted when the focus is to obtain a specific zeolite, which generally occurs by adding chemical reagents as silicon or aluminium sources. The variation in the mass proportion of the above-mentioned precursors is sufficient to adjust the Si/Al ratio, which in theory, is enough to obtain a variety of zeolitic phases, without the need for chemical reagents for Si/Al ratio adjustment. Another advantage is the possibility of using two industrial wastes simultaneously, instead of just one, which can bring greater benefits to the industrial sector in mitigating environmental impacts.

This research was conducted using the combination of GPW and AAW as precursors, aiming at the production of single-phase analcime zeolite. The Placket Burman statistic design was applied to evaluate which synthesis variables investigated in this study present greater statistical relevance, enabling future optimization.

2 Materials and Methods

2.1 Precursor Materials

Glass powder waste (GPW) and aluminium anodizing waste (AAW) were used as precursor materials as sources of silicon and aluminium, respectively, being supplied by Bend Glass Comércio e Indústria LTDA and Akrominas—Comércio de

Table 1 Physicochemical properties of analcime zeolite. Modified from [7, 30]

Chemical formula	Framework structure	Channel dimension (Å)	Cation exchange capacity (meq.g^{-1})	Crystalline system	Space group	Framework density (T/1000 Å^3)
$Na_{16}Al_{16}Si_{32}O_{96}.16H_2O$	ANA	1.6×4.6	4.5	Cubic	*Ia3d*	19.2

Aluminio LTDA, both located in Contagem (Minas Gerais, Brazil). The materials were oven-dried at 100 °C for 48 h and deagglomerated in a porcelain ball mill for 30 min. As a source of alkali, sodium hydroxide in micropellets (reagent grade 98%) was used. During the synthesis, deionized water obtained from reverse osmosis filter (conductivity < 1.5 µS.cm) was used, to avoid any ions that could interfere in the synthesis.

2.2 Materials Characterization

The chemical composition of the GPW and AAW was determined via X-ray fluorescence (XRF) analysis using a Rayny EDX-720 Spectrometer (Shimadzu, US).

The identification of crystalline phases in the samples of precursor materials was performed by X-ray diffraction (XRD) analysis, in an Empyrean X-ray Diffractometer (Malvern Panalytical, UK), operating with Cu k-alpha radiation (40 kV, 30 mA), 2θ ranging from 5 to 90º, at 0.06°/s. The crystalline phases were identified using Match3! software, with Crystallography Open Database (revision. 184,238). The mineralogic identification of the synthesized analcime was performed in the same equipment used for the mineralogical characterization of the precursor materials, although the 2θ and step size were modified. For synthesized analcime, the 2θ range was set from 3 to 50°, at 0.02°/s step, since the characteristic peaks of zeolites occur at low 2θ angles. The crystalline phases were identified using Match3! software, followed by semi-quantification using the Rietveld method. The crystallographic patterns used for crystalline phase identification in synthesized analcime samples were obtained from the International Zeolite Association Database. The crystallinity determination was performed by measuring the ratio between the peak area and the total area in the sample diffractogram, according to Eq. (1) [42, 43].

$$\%crystallinity = \frac{Sum\ of\ cristalline\ peaks\ area}{Total\ area} * 100 \quad (1)$$

The FT-IR analysis of precursor materials and synthesized analcime was performed in an Alpha II Spectrometer (Bruker, DE) in Attenuated Total Reflectance (ATR) mode, with a nominal resolution of 4 cm^{-1}. The spectra were recorded from 4000 to 400 cm^{-1}, and an average of 32 scans were taken.

The size distribution of precursor materials was measured by a Laser Particle Analyzer 1064L (Cilas, FR). The samples were deagglomerated in an ultrasonic bath for 200 s.

Zeta potential measurements were performed using a Zetasizer 3000 HS 1256 (Panalytical, UK). The suspensions were prepared by adding 0.01 g of synthesized analcime in 25 mL of KCl 10^{-3} M solution (supporting electrolyte). Then, the pH (range 1 to 9) was adjusted using dilute solutions of NaOH and HCl, and measurements were performed in triplicate.

Scanning electron microscopy (SEM) was performed using a Quanta 200 FEI microscope (Thermofisher, US), with a resolution of 1.6 nm, operating with 10 to 15 kV. The samples underwent carbon metallization before analysis to provide good electric conductivity.

The thermogravimetry analysis was performed in a DTA60H Thermogravimetric Analyzer (Shimadzu, US), using an aluminium crucible, a heating rate of 10 °C.min^{-1}, with temperature ranging from 25 to 900 °C, and a 50 mL. min^{-1} nitrogen flow.

Nitrogen adsorption/desorption analysis was performed in an Autosorb 1 Gas Sorption analyzer (Quantachrome Instruments, EUA), at a relative pressure of 0.01 to 1.0. The samples were degassed for 24 h at 200 ºC before the analyses. The specific surface area (SSA) was determined from the isotherms obtained at -196 ºC, by applying the multipoint BET (Brunauer–Emmett–Teller) method, whereas pore size distribution of the synthesized analcime was determined using the BJH (Barret-Joyner-Halenda) method. Data processing was conducted using the AsiQwin software.

2.3 Zeolite Synthesis

The synthesis of analcime zeolite from GPW and AAW was conducted in a 2-step process (alkaline fusion followed by hydrothermal synthesis). Initially, a given mass of GPW, AAW, and NaOH was measured on an analytical digital balance, hand-milled to homogenize the mixture, and then calcined in a porcelain crucible. The material resulting from the alkaline fusion was dissolved in deionized water and stirred for 1 h. Then, 20 mL of the solution was transferred to a Teflon-lined stainless-steel autoclave, remaining in an oven for crystallization. At the end of the process, the solid obtained was filtered and washed several times until pH 9 was reached, to remove excess Na^+ ions. Finally, the solid was oven-dried at 60 °C for 24 h.

2.4 Plackett Burman Statistic Design

For the development of this research, 7 experimental variables were considered, based on previous studies, as shown in Table 2. Since this number of variables requires a large number of tests to be conducted, the Plackett Burman statistic design was applied for an initial assessment to identify which variables have greater statistical relevance in the synthesis, allowing the study to run a reduced number of tests [44]. Recent researchers have used this methodology in their studies, obtaining consistent results [45–47]. Thus, 7 variables were combined in a 12-run non-geometric experimental design, as shown in Table 3. The crystallinity (%) and analcime content (%) in the products obtained from the synthesis

Table 2 Variables in the synthesis and their low/high levels

Factors	Symbol	Unit	Levels	
			Low (-1)	High (+1)
Calcination temperature	C_{temp}	°C	500	700
Calcination time	C_{time}	h	2	3
SiO_2/Al_2O_3 molar ratio	SiO_2/Al_2O_3	-	2.5	8
Na_2O/SiO_2 molar ratio	Na_2O/SiO_2	-	6	15
H_2O/Na_2O molar ratio	H_2O/Na_2O	-	200	300
Crystallization temperature	Cr_{temp}	°C	90	110
Crystallization time	Cr_{time}	h	4	24

were defined as response variables. The experimental design was conducted in duplicate, and the mean values of crystallinity (%) and analcime content (%) were taken.

3 Results and Discussion

3.1 Characterization of GPW and AAW

Figure 1 shows the diffractograms obtained from the AAW and GPW samples from XRD analysis. The AAW sample (Fig. 1a) exhibits the absence of an amorphous halo, and high-intensity peaks, revealing the crystalline nature of this material. The peaks observed can be assigned to gibbsite (α-$Al(OH)_3$, COD 9015976) and bayerite (β-$Al(OH)_3$, COD 1000061), isomorphic forms of aluminium hydroxide. The crystalline form of AAW implicates high chemical stability, which impairs the dissolution of the material, and consequently, limits the amount of Al^{3+} in the precursor gel. The GPW diffractogram reveals low-intensity peaks of fluorite (CaF_2, COD 9007064) and quartz (SiO_2,

Table 3 Placket Burman experimental design

Test number	C_{temp}	C_{time}	SiO_2 / Al_2O_3	Na_2O / SiO_2	H_2O / Na_2O	Cr_{temp}	Cr_{time}
1	700	2	8	15	200	110	24
2	500	3	8	6	200	90	24
3	700	3	2.5	6	300	110	24
4	700	3	2.5	6	200	110	4
5	700	2	2.5	15	300	90	24
6	500	2	8	6	300	110	24
7	500	2	2.5	15	200	110	24
8	500	3	8	15	300	110	4
9	700	2	8	6	300	90	4
10	500	3	2.5	15	300	90	4
11	700	3	8	15	200	90	4
12	500	2	2.5	6	200	90	4

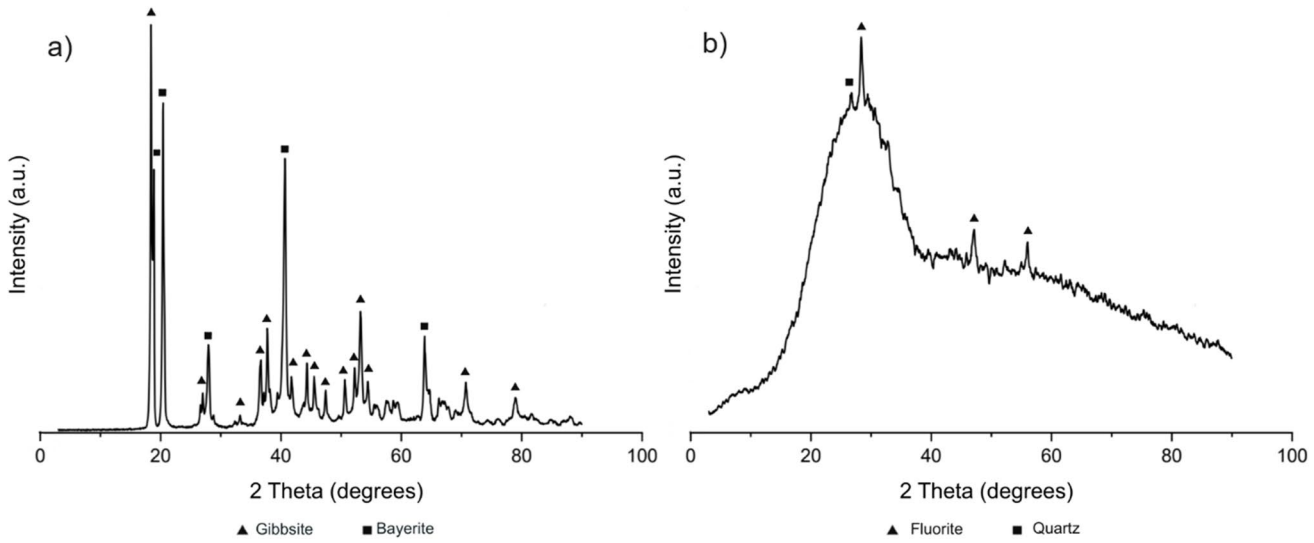

Fig. 1 X-ray diffractograms of AAW (**a**) and GPW (**b**)

COD 1011097), and can be seen in the diffractogram the presence of an amorphous halo (Fig. 1b), which characterizes GPW as an amorphous material. Even though amorphous materials can present high chemical reactivity, glass hardly solubilizes, impairing the liberation of Si^{4+} in the precursor gel. Since the two materials are insoluble in water, it is necessary to subject them to alkaline fusion. In this process, the materials are fused with an alkali reagent, *e.g.,* sodium hydroxide, at temperatures ranging from 500 to 700ºC. The products of this reaction are sodium aluminate and sodium silicate, both soluble species [48].

The GPW and AAW chemical composition and size distribution are described in Table 4. AAW is mainly composed of aluminium and shows a low percentage of other contaminant elements. The FT-IR analysis (to be discussed in detail in the next sections) revealed that the main contaminants present in the sample are sulfur compounds, originating from the acidic bath step present in the anodization process [41]. As verified in the thermogravimetry analysis, the loss on ignition represents 36% of the sample, close to the value obtained via XRF (33.7%). The high temperatures involved in the alkaline fusion can volatilize these compounds and lead to the dehydration of aluminium hydroxides. The GPW is composed of silicon (70.6%) and calcium + sodium (approximately 22%), elements used in the glass fabrication process. The sodium present in GPW acts as a Na^+ source, which can reduce the amount of NaOH needed in the synthesis.

The Si/Al ratio plays a fundamental role in the synthesis of a specific zeolite, directly influencing the crystalline structure, particle morphology and, consequently, the physicochemical properties. As the two residues are sources of silicon and aluminium separately, the Si/Al ratio required for the crystallization of a specific zeolite can be obtained with only these two materials, without the need to add chemical compounds for stoichiometric adjustment, which brings economic benefits into the synthesis process. As the precursor materials are composed mainly of silicon and aluminium, the total mass used in the synthesis can be converted to zeolitic materials, with no generation of co-residue. Comparatively, a high amount of contaminant elements (especially iron) found in other precursor materials (*e.g.*, coal fly ash and metakaolin) leads to the necessity of leaching the silicon and aluminium, and the remaining solid is considered waste [42]. Another possibility for these types of precursors is to use them directly in the synthesis, which leads to the formation of zeolitic materials with low crystallinity and high content of contaminants.

Table 4 also shows the size distribution of the GPW and AAW samples. The medium diameter (D_m) measured for GPW and AAW were 9.0 and 25.4 µm, respectively. The materials fineness is a consequence of its generation (abrasion and precipitation). It is not necessary to grind the material to obtain this size distribution (only to deagglomerate the materials after drying), which results in lower energy consumption. Another advantage is the materials fineness, enabling a more homogeneous mixture with the sodium hydroxide, which favours the chemical reactions in the alkali fusion step.

Table 4 Chemical composition and particle size distribution of GPW and AAW

Chemical composition (%wt)	GPW	AAW
SiO_2	70.6	0.2
Al_2O_3	1.1	64.6
CaO	10.4	-
Cr_2O_3	-	-
Fe_2O_3	0.3	0.3
K_2O	0.2	-
MgO	0.8	-
MnO	-	-
Na_2O	11.9	1.1
P_2O_5	0.3	-
TiO_2	0.1	-
LOI	4.1	33.7
Particle size distribution (µm)		
D_m	9.0	25.4
D_{10}	1.4	4.6
D_{50}	7.8	25.2
D_{90}	21.4	43.4

3.2 Main Variables in the Analcime Synthesis

Table 5 summarizes the coefficients and effects obtained from the Placket Burman statistic design on crystallinity (%) and analcime content (%). Crystallization time (Cr_{time}) and temperature (Cr_{temp}) are the variables with the greatest statistical significance (*p-value* 0.04 and 0.06, respectively) for analcime content (%), positively affecting the response. For crystallinity (%), Cr_{time} and Cr_{temp} were not considered significant (*p-value* 0.14 and 0.13, respectively) since the responses are higher than the 0.05 significance level. However, considering the effect values seen in Table 5, among all variables analyzed in this study, crystallinity (%) is positively affected by Cr_{time} and Cr_{temp}. As verified in Table 6, the tests reaching greater crystallinity are those conducted at the high-level values of time and temperature. In tests conducted at a low level, the products obtained showed lower crystallinity, because the energy supplied is relatively low for the analcime to crystallize properly. At high-level temperatures and low-level time, crystallinity is also impaired, as nuclei begin to form, but there is not enough time for the crystals to grow [14].

Table 5 Summary of coefficients and effects on response variables for 95% confidence level

	Analcime content (%)				Crystallinity (%)			
	Effect	Coef	*t-value*	*p-value*	Effect	Coef	*t-value*	*p-value*
Variables								
C_{temp}	1.80	0.90	0.15	0.89	-6.88	-3.44	-0.82	0.46
C_{time}	18.70	9.35	1.52	0.20	6.53	3.26	0.78	0.48
SiO_2/Al_2O_3	2.63	1.32	0.21	0.84	-4.83	-2.42	-0.58	0.59
Na_2O/SiO_2	27.53	13.77	2.24	0.01	9.10	4.55	1.09	0.34
H_2O/Na_2O	-8.15	-4.08	-0.66	0.54	-11.34	-5.67	-1.36	0.25
Cr_{temp}	36.08	18.04	2.93	0.04	15.77	7.89	1.89	0.13
Cr_{time}	32.67	16.33	2.65	0.06	15.26	7.63	1.83	0.14

Table 6 Crystallinity and phase composition of synthesized products

Test number	Crystallinity (%)	Analcime (%)	Cancrinite (%)	Sodalite (%)	Na-P1 (%)
1	74.9	100.0	0.0	0.0	0.0
2	74.5	85.2	14.9	0.0	0.0
3	72.0	93.0	7.1	0.0	0.0
4	61.9	92.6	0.0	7.5	0.0
5	65.8	97.2	0.0	0.0	2.9
6	65.5	100.0	0.0	0.0	0.0
7	75.4	100.0	0.0	0.0	0.0
8	65.9	100.0	0.0	0.0	0.0
9	12.2	0.0	0.0	0.0	0.0
10	52.8	62.7	0.0	0.0	37.3
11	60.7	100.0	0.0	0.0	0.0
12	54.8	24.0	0.0	0.0	76.0

The Na_2O/SiO_2 ratio shows greater influence for analcime content (%) (*Effect 27.53*) compared to crystallinity (%) (*Effect 9.10*), positively affecting both responses. The amount of Na^+ ions had a strong influence on crystallization, impairing analcime crystallization when present in low concentration in the precursor gel. In research verifying the influence of different mineralizing agents, the authors concluded that a low concentration of Na^+ prevents the crystallization of analcime [27]. As an aluminosilicate, Na^+ ions are present in the analcime crystalline structure, and a minimum concentration is necessary for the structure to crystallize adequately, otherwise, the crystallization of analcime is impaired [49].

The SiO_2/Al_2O_3 ratio is the variable that presented the lowest statistical relevance for crystallinity (%) (*Effect -4.83*) since a wide range of values allows the crystallization of several zeolitic phases, as verified in this study. However, the SiO_2/Al_2O_3 ratio possesses a small positive effect on the analcime content (%) response (*2.63*), since a specific range of SiO_2/Al_2O_3 is required for this zeolitic phase to crystallize. Consequently, for the synthesis of any zeolite, this is an important variable to be considered when seeking the production of a single-phase specific zeolite [42].

The H_2O/Na_2O ratio has a negative effect on the analcime content (%) (*Effect -8.15*), although it affects crystallinity (%) more pronouncedly (*Effect -11.34*). In this case, increasing values of this variable negatively affect both responses. The greater amount of water in the system leads to a lower concentration of Na^+ ions in the precursor gel [50], which, as discussed earlier, inhibits the formation of analcime. In the case of crystallization, the greater dilution of the solution makes the monomers more difficult to nucleate, and consequently, reduces the crystal growth rate [51].

The calcination time (C_{time}) and the calcination temperature (C_{temp}) showed *Effect 18.70 and 1.80*, respectively, for analcime content (%), and *Effect 6.53 and -6.88*, respectively, for crystallinity (%). The melting point of sodium hydroxide is observed at approximately 500 °C, and the conversion of GPW and AAW into soluble Na-salts is possible at this temperature [52, 53]. Thus, it is suggested to use the calcination values of temperature and time presented at lower levels, for energy saving, which contributes to reducing the synthesis cost.

The regression analysis is expressed as a first-order polynomial model to estimate analcime content (%) and crystallinity (%) responses, according to Eqs. (2) and (3). R-squared (R^2 or the coefficient of determination) is a

statistical measure in a regression model that determines the proportion of variance in the dependent variable that can be explained by the independent variable. In other words, r-squared shows how well the data fit the regression model. R-squared can take any values between 0 to 1, and values close to 1 mean the best fit of the regression model. The results presented R^2 of 0.85 for analcime content (%), which suggests that the model relatively fits the data. On the other hand, crystallinity (%) presented R^2 of 0.74, which indicates that the effect of the variables considered in this study on this response must be carefully related. It is important to mention that some of these variables were considered statistically relevant only in the levels considered in this research and should not be extended to different ranges.

$$\begin{aligned} Analcime\ content\ (\%) = & -190 + 0.0090 * C_{temp} + 18.7 * C_{time} \\ & + 0.48 * SiO_2/Al_2O_3 + 3.06 * \frac{Na_2O}{SiO_2} \\ & - 0.082 * H_2O/Na_2O + 1.804 * Cr_{temp} \\ & + 1.633 * Cr_{time} \end{aligned} \quad (2)$$

$$\begin{aligned} Crystallinity\ (\%) = & -1.5 - 0.0344 * C_{temp} + 6.53 * C_{time} \\ & - 0.88 * SiO_2/Al_2O_3 \\ & + 1.011 * \frac{Na_2O}{SiO_2} - 0.1134 * H_2O/Na_2O \\ & + 0.789 * Cr_{temp} + 0.763 * Cr_{time} \end{aligned} \quad (3)$$

3.3 Analcime Characterization

Figures 2 and 3 show the XRD results for the products obtained in all tests, and Table 6 summarizes the results

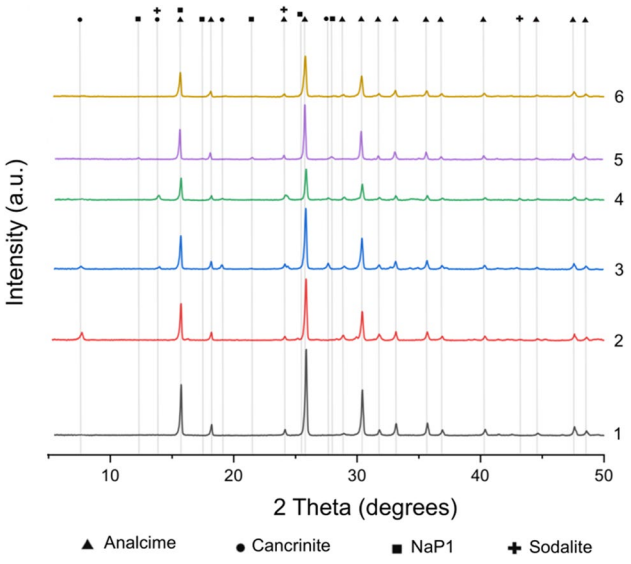

Fig. 2 XRD results of products obtained in tests 1 to 6

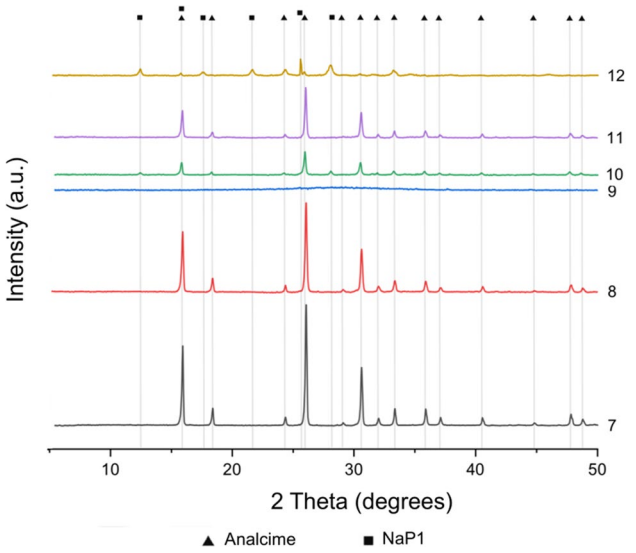

Fig. 3 XRD results of products obtained in tests 7 to 12

of crystallinity and mineralogic composition obtained by Rietveld refinement in each test. The goal of synthesizing single-phase analcime zeolite was achieved in most tests, especially tests 1 and 7, and in addition to purity, the synthesized analcime showed high crystallinity, due to the absence of an amorphous halo. Analcime, cancrinite ($Na_6CaCO_3[Al_6Si_6O_{24}]0.2H_2O$, CAN framework), sodalite ($Na_8Cl_2[Al_6Si_6O_{24}]$, SOD framework) and Na-P1 ($Ca_4[Al_8Si_8O_{32}]0.16H_2O$, GIS framework) are the phases competing during crystallization, making the definition of limits for the experimental variables of great importance to obtain single phase analcime zeolite. It is reported in the literature that the optimum crystallization time for analcime is approximately 24 h [54]. Although the temperature was indicated to be set at 200 °C [55], in this research it was possible to obtain single phase analcime at 110 °C. According to the XRD results, the formation of Na-P1 zeolite was verified in tests 5, 10, and 12, which have lower crystallization temperature values. As verified by [56], the crystallization of GIS framework can be achieved at temperatures of 90 °C, and above 100 °C the formation of a mixture of GIS framework and analcime was verified, according to the results obtained in the present study. Despite the formation of two phases, due to the short crystallization time, in the aforementioned tests, the crystallinity observed was relatively low [56].

Despite the goal of crystallizing only analcime zeolite in this work, the crystallization of other types of zeolites can be considered positive, since it reveals the potential of the combination between GPW and AAW for zeolite synthesis, which increases the possibility of using these materials as precursors. For test 9, the experimental conditions were inadequate for the crystallization of any type of zeolite, and the product showed markedly low crystallinity.

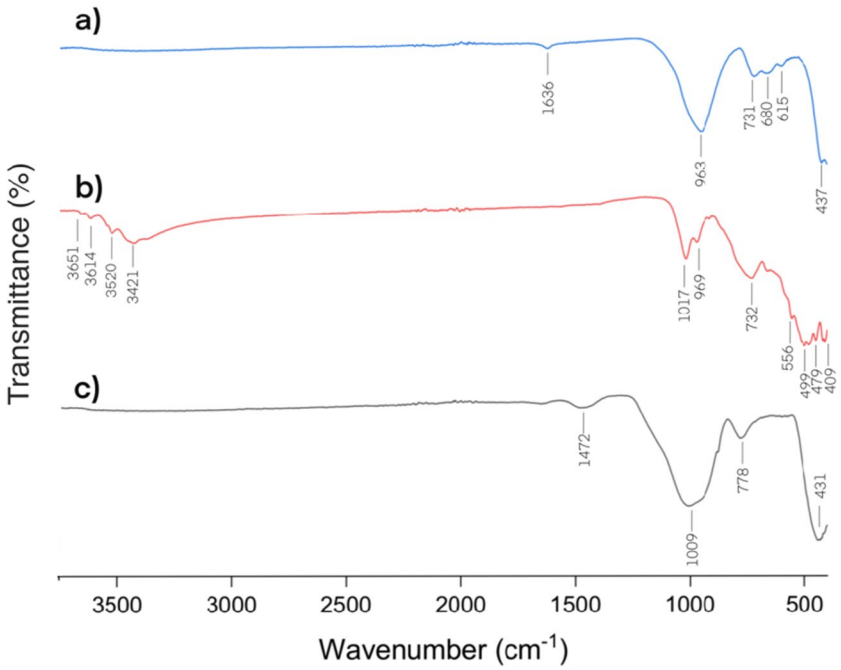

Fig. 4 FT-IR spectra of (**a**) the synthesized analcime, (**b**) aluminium anodizing waste, and (**c**) glass powder waste

According to the results shown in Table 6, the highest crystallinity was observed in test 7, and this sample was subjected to further characterization by FT-IR analysis, zeta potential measurement, scanning electron microscopy, thermogravimetry and nitrogen adsorption–desorption.

The FT-IR spectrum of the synthesized analcime is shown in Fig. 4a. The bands located at 437 cm^{-1} and 615 cm^{-1} indicate the T-O-T bending vibration, where T represents Si and/or Al [54, 57]. Symmetric stretching is represented by the band at 680 cm^{-1} and 731 cm^{-1} [54]. The spectrum exhibits an intense peak at 936 cm^{-1}, a striking feature of zeolitic materials, representing asymmetric stretching vibration of T-O-T bonds [42]. It can also be seen a low-intensity peak at 1636 cm^{-1}, which is related to the bending vibration of O–H bonds, due to the presence of water molecules inside the zeolite micropores [42, 58]. Figure 4b shows the FT-IR spectrum of aluminium anodizing waste. The bands located at 3651, 3614, 3520, 3421, 732, and 556 cm^{-1} are related to O–H stretching and bending vibrations, characteristic of bayerite and gibbsite phases. Bands observed in the 1017 and 969 cm^{-1} are related to the S–O vibration, of the aluminium sulfate hydrate. The sulfur content in the sample makes up the volatile substances the AAW, present as a loss on ignition as verified in the XRF and thermogravimetry analysis. The bands located at 556, 499, 479 and 409 are related to Al-O stretching bonds [41, 59, 60]. The FT-IR of GPW is also presented, in Fig. 4c. The peak observed at 1472 cm^{-1} is related to O–H stretching vibrations, due to water molecules present in the sample. The intense peak observed at 1009 cm^{-1} can be associated with the Si–O-Si and Si–O stretching vibration, whereas the asymmetric vibration of Si–O-Si is represented by the peak at 431 cm^{-1}. The symmetric stretching vibration of Si–O bonds is identified by the 778 cm^{-1} peak [61]. It can be seen, due to the absence of characteristic peaks of GPW and AAW and the appearance of new peaks in the synthesized analcime, that the precursor materials were successfully converted into zeolitic material, in agreement with the XRD analysis.

Figure 5 illustrates the zeta potential results for the synthesized analcime in the pH range from 1 to 9. The synthesized analcime displays a negative electrical charge in a wide pH range. The natural negative charge is enhanced in the alkaline solution due to the presence of an excess of OH^- [62], with a maximum value of -47.3 mV at pH 9.0.

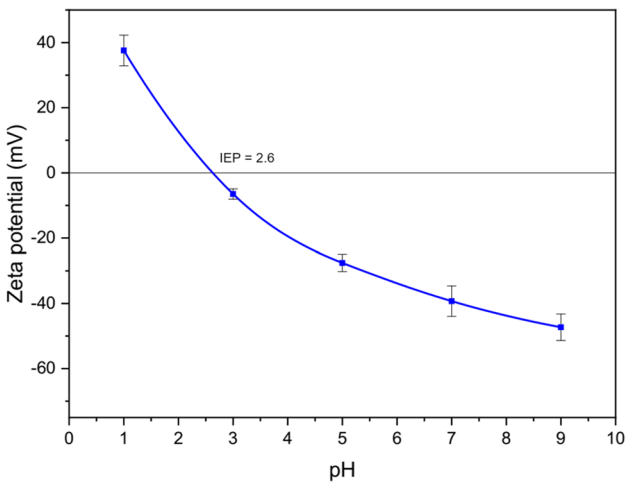

Fig. 5 Zeta potential of synthesized analcime

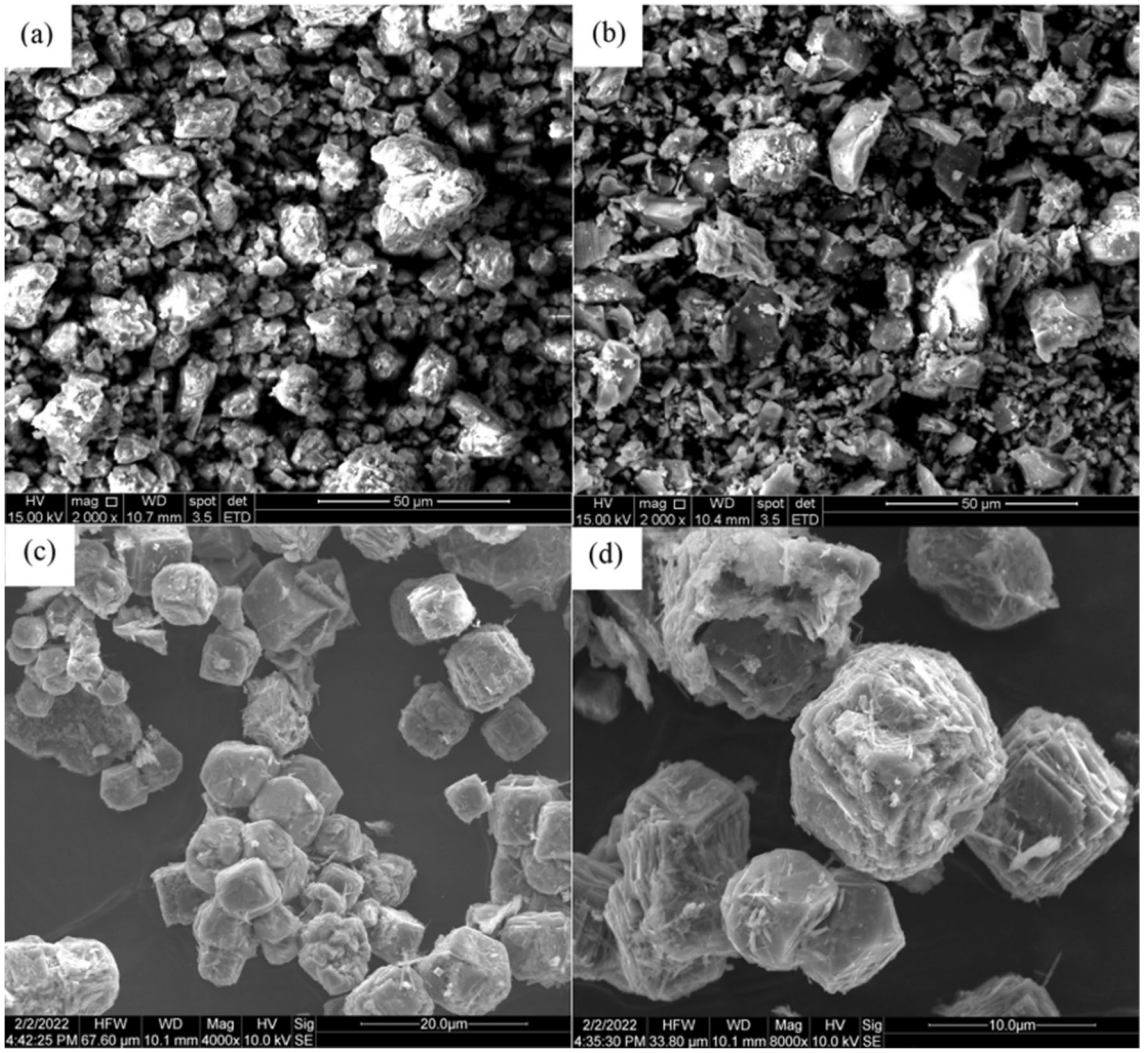

Fig. 6 SEM images of the precursor materials AAW (**a**) and GPW (**b**), and the synthesized analcime zeolite (**c**) and (**d**)

The isoelectric point (IEP) is observed at approximately pH 2.6. Below this pH, in a strongly acidic solution, the analcime particles became positively charged, due to an excess of H^+ [62], with a maximum value of 37.6 mV at pH 1.0. The IEP determination is of great importance in the application of low-silica zeolite (as in the case of analcime) as an adsorbent material for contaminant removal from wastewater. Zeolites can readily remove cationic species due to electrostatic attraction (*e.g.*, heavy metals, ammonia, and dyes), but removing anionic species is hardly possible. However, pH values below the IEP can enable the removal of anionic species due to induced positive electrical charge [63–69]. Hence, the IEP determination for any zeolite is of fundamental importance for the treatment of effluents contaminated by anionic species, which amplifies the possibility of applying this material as an adsorbent to water and wastewater treatment. Besides, the increment in the negative electrical charge in the high pH levels can increase the efficiency of analcime in the removal of cationic species [70]. However, it is important do mention that in acidic conditions part of aluminium atoms can be removed from the framework, process known as dealumination. Several methods of dealumination are used, including treatment with organic and inorganic acids. The increase of Si/Al ratio from dealumination can lead to larger pores and reduction of cation exchange capacity [71], and the application of zeolites to remove anionic species in strongly acidic environment should be carefully evaluated.

SEM images of the precursor materials and analcime are shown in Fig. 6. The AAW particles (Fig. 6a) present rough surfaces that may be related to the precipitation of $Al(OH)_3$ in the formation by precipitation of the anodizing waste. As for GPW (Fig. 6b), the cutting and polishing of glass pieces result in the formation of sharp-edged particles. Both materials exhibit a wide particle size distribution, consistent with the particle size analysis in terms of their D_{90} and

D_{10} (1.4 and 21.4µ, respectively, for GPW, 4.6 and 43.4 µm, respectively, for AAW). In contrast, visually, analcime particles present a relatively uniform particle size distribution (Fig. 6c), with particles of approximately 10 µm. This particle size was also observed by other authors, in the synthesis of analcime from kaolin [72, 73]. In Fig. 6d it can be visualized the presence of particles in the form of tetrahedrons, characteristic of analcime, and this morphology was verified in previous studies [26, 28, 54].

The thermogravimetric curves of GPW, AAW and synthesized analcime are shown in Fig. 7. For GPW, the total mass loss observed is about 5%. The mass reduction of approximately 4% observed in the first region up to 200 °C is related to the elimination of water adsorbed on particle surfaces. This residue shows great thermal stability, and approximately 1% mass loss is observed until the temperature reaches 900 °C. For the AAW, the total mass loss observed was 36%, which occurred in three steps. The initial 1% in the first step is related to the removal of water adsorbed on particle surfaces, followed by a significant mass loss up to approximately 600 °C. In the second step, located in the 200–350 °C range, the mass loss of approximately 27% is related to the dehydration of $Al(OH)_3$, followed by approximately 7% mass loss in the third region, from 350° to 600 °C, that can be associated with the elimination of aluminium sulfate hydrates [41], confirmed by the FT-IR analyses. Above 600 °C, less than 1% mass loss is observed. For synthesized analcime, mass loss can also be observed in three steps, due to different energy involved in the diffusion of desorbed water molecules [69]. In the first region, from 25° to 200 °C, the analysis shows a slight mass loss of 4%, related to the water molecules adsorbed on the surface of the particles, followed by a significant mass loss of approximately 8% in the second region, up to 450 °C, that correspond to the removal of occluded water molecules. Above 450 up to 900 °C, a mass loss of approximately 3% is observed, related to the gradual removal of water trapped inside the micropores [69]. The total mass loss in synthesized analcime is about 15%, which is consistent with values observed for analcime found in the literature [25, 54, 68, 69].

Figure 8 shows the nitrogen adsorption–desorption isotherms obtained for the synthesized analcime. Zeolites are crystalline materials classified as microporous materials (with pores less than 2 nm), although, in this study, the isotherm obtained shows a type-IV behaviour, suggesting that the sample does not exhibit a significant presence of micropores. The presence of a H3-type hysteresis is noticed above 0.40 (P/P_0), which indicates the presence of mesopores (2 to 50 nm) [43]. Figure 8 also shows the pore size distribution of the synthesized analcime. It is observed that the sample exhibited pores in the 3–30 nm range, dominated by 5 nm pores, which can be associated with the interparticle spaces present in the synthesized analcime. Table 7 shows

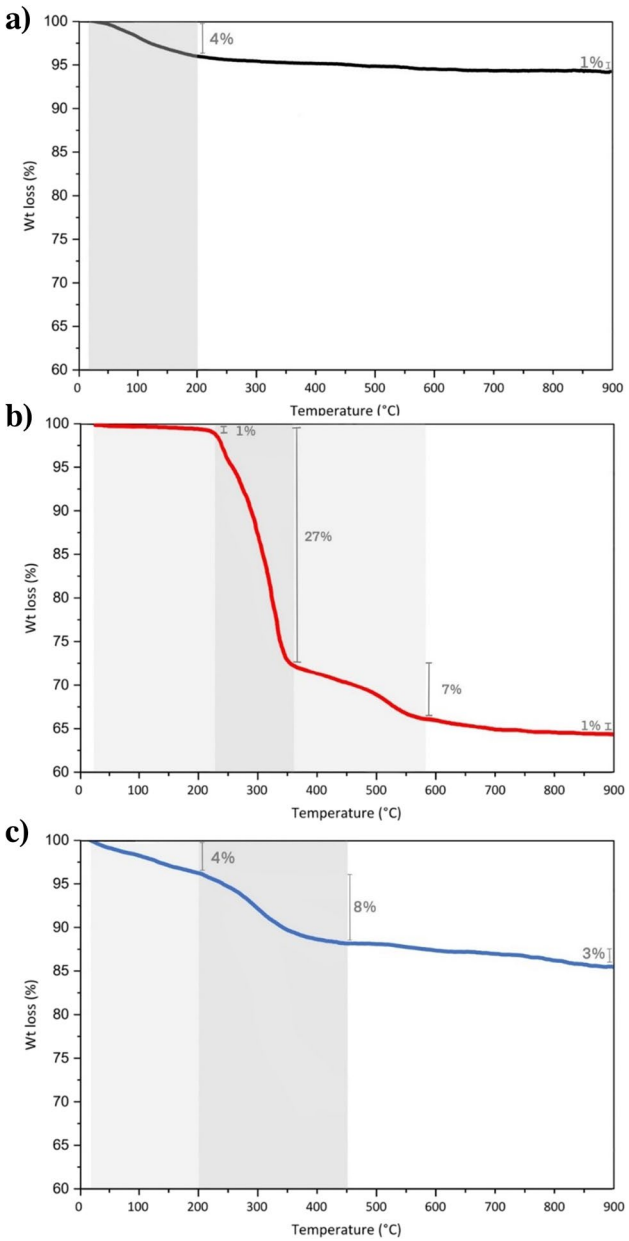

Fig. 7 Synthesized GPW (**a**), AAW (**b**) and synthesized analcime (**c**) thermogravimetric (TG) curves

the specific surface area (SSA) of the precursor materials and the synthesized analcime obtained in this study, including those obtained from other industrial wastes for comparison purposes. The synthesized analcime exhibits SSA of 43.3 $m^2.g^{-1}$, whereas the precursor materials, GPW and AAW, exhibit SSA of 4.3 and 6.1 $m^2.g^{-1}$, respectively. The expressive increase in the SSA is related to the formation of a porous crystalline structure, with interconnected pores and channels. In comparison to the analcime synthesized from

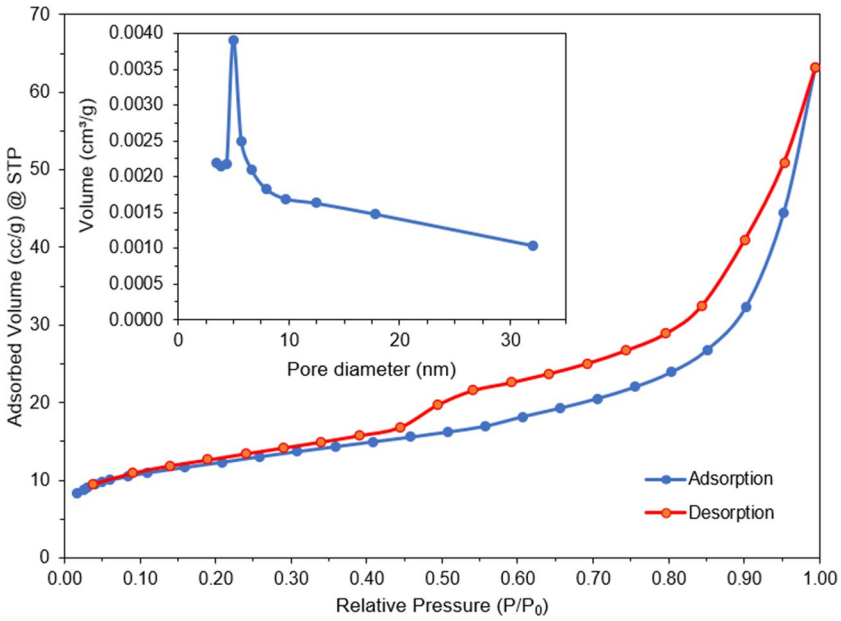

Fig. 8 Synthesized analcime nitrogen adsorption–desorption isotherms and pore size distribution

Table 7 Specific surface area of GPW, AAW, and synthesized analcime obtained by different industrial residues

Materials	Specific surface area ($m^2.g^{-1}$)	References
Glass powder waste	4.3	This study
Aluminium anodizing waste	6.1	This study
Analcime synthesized from GPW and AAW	43.3	This study
Analcime synthesized from fly ash	8.0	[43]
Analcime synthesized from perlite	18.9	[70]
Analcime synthesized from coal gangue	17.0	[74]

different precursor materials by other researchers, it can be noticed that the SSA obtained in this study is significantly superior. Other materials used have a considerable quantity of contaminant elements in their chemical composition, *e.g.* iron, magnesium, and calcium, resulting in zeolites with low crystallinity, and consequently, low SSA. Since the GPW and AAW used as precursors are mainly composed of silicon and aluminium, the product obtained in the synthesis is highly crystalline, displaying superior specific surface area, which may increase the possibility of use in different applications.

4 Conclusions

In this work, single-phase analcime with high crystallinity was synthesized from the combination of glass powder waste and aluminium anodizing waste. Due to precursor materials insolubility, a 2-step approach was used, *i.e.,* alkaline fusion followed by hydrothermal synthesis. From the results obtained by the Plackett Burman statistic design, crystallization temperature and crystallization time were observed to be the variables with the greatest statistical relevance in the formation of analcime content (%), whereas alkaline fusion temperature and time presented the least relevance for analcime content (%) and crystallinity (%). The synthesized analcime obtained showed crystallinity up to 75%, although the results indicated that the optimization of the variables may lead to the formation of pure analcime with higher crystallinity. The characterization of the product obtained revealed a material with a specific surface area of 43.3 $m^2.g^{-1}$, larger than those of analcime samples synthesized from other precursor materials. The synthesized analcime possesses an average pore size of 5 nm, consistent with the theoretical analcime pore size. Zeta potential analysis indicates the zeolite presents an IEP at pH 2.6, important information in the case of an application for the removal of anionic species in wastewater treatment. Thermogravimetry, FT-IR, and SEM analysis confirmed the conversion of the precursor materials, in agreement with the results obtained from XRD analysis. The results indicate that obtaining zeolites, especially analcime, for application in various industrial sectors is an alternative for the reuse of GPW and AAW, adding value to these residues, and contributing to sustainability and a circular economy.

Acknowledgements The authors acknowledge Pró-Reitoria de Pesquisa (PRPq – Universidade Federal de Minas Gerais), CNPq, FAPEMIG, CAPES, and PROEX CAPES for their support of PPGEM.

Author's contribution L. F. de Magalhães worked on conceptualization, methodology, formal analysis, investigation, data curation, software,

writing – original draft, writing – review & editing, visualization and preparation of figures and tables; G. R. da Silva contributed with writing – review & editing, supervision, project administration; V. A. A. de Freitas workes on writing – review & editing; A. B. Henriques contributions was in investigation and A. E. C. Peres contributed with supervision.

Funding This study was financed in part by Coordenação de Aperfeiçoamento de Pessoal de Nível Superior – Brasil (CAPES) – Finance Code 001.

Data Availability The data that support the findings of this study may be available from the corresponding author request.

Declarations

Ethics Approval Not applicable.

Consent to Publication I confirmed.

Consent to Participate I confirmed.

Competing Interests The authors declare no competing interests.

References

1. Sivalingam S, Sen S (2018) Appl Surf Sci 455. https://doi.org/10.1016/j.apsusc.2018.05.222
2. Yao G, Lei J, Zhang X, Sun Z, Zheng S, Komarneni S (2018) Mater Res Bull 107. https://doi.org/10.1016/j.materresbull.2018.07.021
3. Alves JABLR, Dantas ERS, Pergher SBC, Melo DMA, Melo MAF (2013) Mater Res 17. https://doi.org/10.1590/s1516-14392013005000191
4. Chen J, Huang R, Ouyang H, Yu G, Liang Y, Zheng Q (2021) J Clean Prod 320. https://doi.org/10.1016/j.jclepro.2021.128861
5. Vidal CB, Raulino GS, Barros AL, Lima AC, Ribeiro JP, Pires MJ, Nascimento RF (2012) J Environ Manage 112. https://doi.org/10.1016/j.jenvman.2012.07.026
6. Xie WM, Zhou FP, Bi XL, Chen DD, Li J, Sun SY, Liu JY, Chen XQ (2018) J Hazard Mater 358. https://doi.org/10.1016/j.jhazmat.2018.07.007
7. de Magalhães LF, da Silva GR, Peres AEC (2022) Adsorpt Sci Technol 2022. https://doi.org/10.1155/2022/4544104
8. Cardoso AM, Horn MB, Ferret LS, Azevedo CM, Pires M (2015) J Hazard Mater 287. https://doi.org/10.1016/j.jhazmat.2015.01.042
9. Koohsaryan E, Anbia M, Maghsoodlu M (2020) J Environ Chem Eng 8. https://doi.org/10.1016/j.jece.2020.104287
10. Collins F, Rozhkovskaya A, Outram JG, Millar GJ (2020) Microporous Mesoporous Mat 291. https://doi.org/10.1016/j.micromeso.2019.109667
11. Li Y, Li L, Yu J (2017) Chem 3. https://doi.org/10.1016/j.chempr.2017.10.009
12. Kosinov N, Gascon J, Kapteijn F, Hensen EJM (2016) J Membr Sci 499. https://doi.org/10.1016/j.memsci.2015.10.049
13. Kumar S, Srivastava R, Koh J (2020) J CO2 Util 41. https://doi.org/10.1016/j.jcou.2020.101251
14. Qiang Z, Shen X, Guo M, Cheng F, Zhang M (2019) Microporous Mesoporous Mat 287. https://doi.org/10.1016/j.micromeso.2019.05.062
15. Khodaverdi E, Soleimani HA, Mohammadpour F, Hadizadeh F (2016) Chem Biol Drug Des 87. https://doi.org/10.1111/cbdd.12716
16. Vilaca N, Amorim R, Machado AF, Parpot P, Pereira MF, Sardo M, Rocha J, Fonseca AM, Neves IC, Baltazar F (2013) Colloids Surf B Biointerfaces 112. https://doi.org/10.1016/j.colsurfb.2013.07.042
17. Das M, Adhikary SK, Rudzionis Z (2022) Mater Today Proc 61. https://doi.org/10.1016/j.matpr.2021.09.005
18. Kaplan G, Coskan U, Benli A, Bayraktar OY, Kucukbaltacı AB (2021) Constr Build Mater 311. https://doi.org/10.1016/j.conbuildmat.2021.125336
19. Tran YT, Lee J, Kumar P, Kim K-H, Lee SS (2019) Compos B Eng 165. https://doi.org/10.1016/j.compositesb.2018.12.084
20. Bish DL, Ming DW (2001) Natural zeolites: occurrence, properties, applications. Mineralogical Society of America, Washington D.C
21. Masters AF, Maschmeyer T (2011) Microporous Mesoporous Mat 142. https://doi.org/10.1016/j.micromeso.2010.12.026
22. Bartlocher C, McCusker LB, Olson DH (2007) Atlas of zeolite framework types, 6th edn. Elsevier, Amsterdam
23. Colella C, Wise WS (2014) Microporous Mesoporous Mat 189. https://doi.org/10.1016/j.micromeso.2013.08.028
24. Indira V, Abhitha K (2022) Energy Nexus 7. https://doi.org/10.1016/j.nexus.2022.100095
25. Vereshchagina TA, Kutikhina EA, Solovyov LA, Vereshchagin SN, Mazurova EV, Chernykh YY, Anshits AG (2018) Microporous Mesoporous Mat 258. https://doi.org/10.1016/j.micromeso.2017.09.011
26. Vigil de la Villa Mencía R, Goiti E, Ocejo M, Giménez RG (2020) Microporous Mesoporous Mat 293. https://doi.org/10.1016/j.micromeso.2019.109817
27. Hsiao Y-H, Ho T-Y, Shen Y-H, Ray D (2017) Appl Clay Sci 143. https://doi.org/10.1016/j.clay.2017.04.014
28. Bortolini HR, Lima DS, Perez-Lopez OW (2020) J Cryst Growth 532. https://doi.org/10.1016/j.jcrysgro.2019.125424
29. Bejar A, Ben Chaabene S, Jaber M, Lambert J-F, Bergaoui L (2014) Microporous Mesoporous Mat 196. https://doi.org/10.1016/j.micromeso.2014.05.004
30. Baerlocher C, McCusker LB. Database of Zeolite Structures, Structure Commission of the International Zeolite Association, http://asia.iza-structure.org/IZA-SC/ftc_table.php. Accessed in 13/12/2022
31. He Y, Tang S, Yin S, Li S (2021) J Clean Prod 306. https://doi.org/10.1016/j.jclepro.2021.127248
32. Ma Y, Yan C, Alshameri A, Qiu X, Zhou C, Li D (2014) Adv Powder Technol 25. https://doi.org/10.1016/j.apt.2013.08.002
33. Khan MNN, Kuri JC, Sarker PK (2021) J Build Eng 34. https://doi.org/10.1016/j.jobe.2020.101934
34. Dadsetan S, Siad H, Lachemi M, Sahmaran M (2021) J Clean Prod 278 https://doi.org/10.1016/j.jclepro.2020.123983
35. Du Y, Yang W, Ge Y, Wang S, Liu P (2021) J Clean Prod 287. https://doi.org/10.1016/j.jclepro.2020.125018
36. Kalakada Z, Doh J-H, Chowdhury S (2019) Eur J Environ Civ 26. https://doi.org/10.1080/19648189.2019.1695149
37. Ramteke DD, Hujova M, Kraxner J, Galusek D, Romero AR, Falcone R, Bernardo E (2021) J Clean Prod 278. https://doi.org/10.1016/j.jclepro.2020.123985
38. Salzmann RD, Ackerman JN, Cicek N (2022) Environ Technol 43. https://doi.org/10.1080/09593330.2020.1775711
39. Mymrin V, Pedroso DE, Pedroso C, Alekseev K, Avanci MA, Winter E, Cechin L, Rolim PHB, Iarozinski A, Catai RE (2018) J Clean Prod 174. https://doi.org/10.1016/j.jclepro.2017.10.299
40. Souza MT, Onghero L, Repette WL, Raupp Pereira F, de Oliveira APN (2020) J Build Eng 30. https://doi.org/10.1016/j.jobe.2020.101233

41. Souza MT, Simao L, Montedo ORK, Raupp Pereira F, de Oliveira APN (2019) Waste Manag 84. https://doi.org/10.1016/j.wasman.2018.12.003
42. Iqbal A, Sattar H, Haider R, Munir S (2019) J Clean Prod 219. https://doi.org/10.1016/j.jclepro.2019.02.066
43. Kumar MM, Jena H (2022) Microporous Mesoporous Mat 333. https://doi.org/10.1016/j.micromeso.2022.111738
44. Plackett RL, Burman JP (1946) Biometrika 33. https://doi.org/10.2307/2332195
45. Caroca E, Serrano A, Borja R, Jimenez A, Carvajal A, Braga AFM, Rodriguez-Gutierrez G, Fermoso FG (2021) Waste Manag 120. https://doi.org/10.1016/j.wasman.2020.11.027
46. Paul T, Sinharoy A, Pakshirajan K, Pugazhenthi G (2020) J Water Proc Eng 37. https://doi.org/10.1016/j.jwpe.2020.101462
47. Silva JAD, AFM Braga, Fermoso FG, Zaiat M, Silva GHR (2021) J Environ Manage 294. https://doi.org/10.1016/j.jenvman.2021.113002
48. Akın SŞ, Kirdeciler SK, Kazanç F, Akata B (2021) Microporous Mesoporous Mat 325. https://doi.org/10.1016/j.micromeso.2021.111338
49. Yuan J, Yang J, Ma H, Liu C (2016) Microporous Mesoporous Mat 222. https://doi.org/10.1016/j.micromeso.2015.10.020
50. Bai S-x, Zhou L-m, Chang Z-b, Zhang C, Chu M (2018) Carbon Resour Convers 1. https://doi.org/10.1016/j.crcon.2018.08.005
51. Lin Y-J, Chen J-C (2021) J Environ Chem Eng 9. https://doi.org/10.1016/j.jece.2021.106549
52. Mori H (2003) J Mater Sci 38. https://doi.org/10.1023/A:1025100901693
53. Rahaman MA, Gafur MA, Kurny ASW (2013) Am J Mater Eng Technol 1. https://doi.org/10.12691/materials-1-3-6
54. Jiménez A, Misol A, Morato Á, Rives V, Vicente MA, Gil A (2021) J Clean Prod 297. https://doi.org/10.1016/j.jclepro.2021.126667
55. Mintova S, Barrier N (2016) Verified syntheses of zeolitic materials, 3 ed., Elsevier
56. Azizi SN, Daghhigh AA, Abrishamkas M (2013) Phase transformation of zeolite P to Y and analcime zeolites due to changing the time and temperature. J Spectrosc. https://doi.org/10.1155/2013/428216
57. Abdelrahman EA, Alharbi A, Subaihi A, Hameed AM, Almutairi MA, Algethami FK, Youssef HM (2020) J Mater Res Technol 9. https://doi.org/10.1016/j.jmrt.2020.05.052
58. Azizi SN, Ghasemi S, Derakhshani-mansoorkuhi M (2016) Int J Hydrog Energy 41. https://doi.org/10.1016/j.ijhydene.2016.08.181
59. da Silva Nuernberg NB, Niero DF, Bernardin AM (2021) J Clean Prod 298. https://doi.org/10.1016/j.jclepro.2021.126770
60. Jayashree P, Straffelini G (2022) Tribol Int 173. https://doi.org/10.1016/j.triboint.2022.107676
61. Ming NC, Putra Jaya R, Awang H, Siaw Ing NL, Mohd Hasan MR, Al-Saffar ZH (2022) Phys Chem Earth Parts A/B/C 128. https://doi.org/10.1016/j.pce.2022.103263
62. Pugazhenthi G, Vinoth Kumar R (2017) J Water Reuse Desalin 7. https://doi.org/10.2166/wrd.2016.096
63. Adam MR, Salleh NM, Othman MHD, Matsuura T, Ali MH, Puteh MH, Ismail AF, Rahman MA, Jaafar J (2018) J Environ Manage 224. https://doi.org/10.1016/j.jenvman.2018.07.043
64. Arslan A, Veli S (2012) J Taiwan Inst Chem Eng 43. https://doi.org/10.1016/j.jtice.2011.11.003
65. Khanmohammadi H, Bayati B, Rahbar-Shahrouzi J, Babaluo A-A, Ghorbani A (2019) J Environ Chem Eng 7. https://doi.org/10.1016/j.jece.2019.103040
66. PM Nekhunguni, NT Tavengwa, H Tutu (2017) J Environ Manage 197. https://doi.org/10.1016/j.jenvman.2017.04.038
67. Sivalingam S, Sen S (2019) J Taiwan Inst Chem Eng 96. https://doi.org/10.1016/j.jtice.2018.10.032
68. Jing Z, Cai K, Li Y, Fan J, Zhang Y, Miao J, Chen Y, Jin F (2017) J Nucl Mater 488. https://doi.org/10.1016/j.jnucmat.2017.03.008
69. Novembre D, Gimeno D (2021) Sci Rep 11. https://doi.org/10.1038/s41598-021-92862-0
70. Dyer A, Tangkawanit S, Rangsriwatananon K (2004) Microporous Mesoporous Mat 75. https://doi.org/10.1016/j.micromeso.2004.07.007
71. Koohsaryan E, Anbia M (2016) Chinese J Catal 37. https://doi.org/10.1016/S1872-2067(15)61038-5
72. Hegazy EZ, Abd El Maksod IH, Abo El Enin RMM (2010) Appl Clay Sci 49. https://doi.org/10.1016/j.clay.2010.04.019
73. Jamil TS, Youssef HF (2016) Sep Sci Technol 52. https://doi.org/10.1080/01496395.2016.1229337
74. Jin Y, Liu Z, Han L, Zhang Y, Li L, Zhu S, Li ZPJ, Wang D (2022) J Hazard Mater 423. https://doi.org/10.1016/j.jhazmat.2021.127027